

MAMBO Observations at 240GHz of optically obscured *Spitzer* sources: source clumps and radio activity at high redshift

P. Andreani^{1,2}, M. Magliocchetti^{3,4}, G. De Zotti^{5,4}

¹ ESO, Karl-Schwarzschild-Str.2, D-85748, Garching, Germany

² INAF, Osservatorio Astronomico di Trieste, Via Tiepolo 11, I-34143, Trieste, Italy

³ INAF, IFSI, via Fosso del Cavaliere 1100, Roma, Italy

⁴ SISSA, Via Beirut 4, I-34014, Trieste, Italy

⁵ INAF, Osservatorio Astronomico di Padova, Vicolo dell'Osservatorio 5, I-35122 Padova, Italy

12 November 2018

ABSTRACT

Optically very faint ($R > 25.5$) sources detected by the *Spitzer* Space Telescope at $24\mu\text{m}$ represent a very interesting population at redshift $z \sim [1.5 - 3]$. They exhibit strong clustering properties, implying that they are hosted by very massive halos, and their mid-IR emission could be powered by either dust-enshrouded star-formation and/or by an obscured AGN. We report observations carried out with the MAMBO array at the IRAM 30m antenna on Pico Veleta of a candidate protocluster with five optically obscured sources selected from the $24\mu\text{m}$ *Spitzer* sample of the First Look Survey. Interestingly, these sources appear to lie on a high density filament aligned with the two radio jets of an AGN. Four out of five of the observed sources were detected. We combine these measurements with optical, infrared and radio observations to probe the nature of the candidate protocluster members. Our preliminary conclusions can be summarized as follows: the Spectral Energy Distributions of all sources include both AGN and starburst contributions; the AGN contribution to the bolometric luminosities ranges between 14 and 26% of the total. Such a contribution is enough for the AGN to dominate the emission at 5.8, 8 and $24\mu\text{m}$, while the stellar component, inferred from SED fitting, prevails at 1.25mm and at $\lambda < 4.5\mu\text{m}$. The present analysis suggests a coherent interplay at high- z between extended radio activity and the development of filamentary large-scale structures.

Key words: Galaxies: evolution, high redshift, ISM, clusters: general – ISM: general

1 INTRODUCTION

Optically obscured $24\mu\text{m}$ *Spitzer* sources are among the most strongly clustered objects in the Universe. Magliocchetti et al. (2007) studied a complete sample of 793 optically faint ($R > 25.5$) sources with $F_{24\mu\text{m}} \geq 0.35$ mJy, drawn from the *Spitzer* Space Telescope First Look Survey (FLS) (Fadda et al. 2006). Their two-point correlation function has an amplitude $A = (7 \pm 2) \cdot 10^{-3}$ [$w(\theta) = A\theta^{-0.8}$, with θ in degrees], which is about a factor of 8 larger than that obtained for the whole *Spitzer* $F_{24\mu\text{m}} \geq 0.35$ mJy sample (see Fig. 6 of Magliocchetti et al. 2007). Their optical/mid-IR colours indicated that they are ultraluminous far-infrared galaxies at $z \simeq 1.6 - 2.7$, a conclusion supported by redshift determinations based on infrared spectroscopy (IRS; e.g., Yan et al. 2005, 2007; Houck et al. 2005; Weedman et al. 2006a, Desai et al., 2007) and

by comparisons with models for galaxy formation and evolution (e.g., Granato et al. 2004). Their 3D comoving clustering radius was estimated to be $r_0 = [15.2^{+2.3}_{-2.6}]$ Mpc [$\xi(r) = (r/r_0)^{-1.8}$] (Magliocchetti et al. 2007).

Clustering results obtained on Bootes and UKIDSS fields by Brodwin et al. (2008) and Magliocchetti et al. (2008b) based on spectroscopic and photometric $N(z)$ converge, within the errors, at giving similar high clustering lengths and halo masses (r_0 about 13 Mpc and masses $10^{12.5-10^{13}} M_\odot$ for $S > 0.4$ mJy)¹. These measured clustering properties indicate that these sources are associated to very mas-

¹ Note that the clustering length given by Magliocchetti et al. (2008b) is in Mpc for $h = 0.7$, not in h^{-1} Mpc, as stated by Brodwin et al. (2008)

sive dark matter (DM) halos, consistent with them inhabiting the progenitors of groups/clusters of galaxies. Thus, these objects are important tools to investigate the abundance of very massive halos at high z and the evolution of large scale structure.

Bright, high- z QSOs, powered by the most massive black-holes (BHs), display similar clustering properties (Shen et al. 2007) and should therefore inhabit similar halos at $z \sim 2$. Obscured $24\mu\text{m}$ sources in the environment of bright QSOs (and/or radiogalaxies) at $z \sim 2$ then likely trace the largest density peaks and thus the very most massive DM halos. This could be materialized by several filaments crossing at their position. High- z radiogalaxies proved to be particularly effective tracers of distant large scale overdensities that may collapse to form present-day massive clusters of galaxies (Pentericci et al. 1997; Venemans et al. 2007; Overzier et al. 2007; Miley & De Breuck 2008). Since both optically obscured $24\mu\text{m}$ Spitzer sources and high- z radiogalaxies are preferentially found within the rare large-scale, large-amplitude peaks in the primordial density fluctuation field, it is interesting to investigate possible links between these two source populations.

A by-product of the clustering analysis by Magliocchetti et al. (2007) was the discovery of several galaxy alignments, reminiscent of the high- z filaments found in numerical simulations which describe the evolution of large-scale structure. In some cases, the candidate filaments were aligned with radio jets, consistent with West's (1994) prediction that the radio axes reflect the developing large-scale clustering pattern in the early Universe. If so, these systems would be an important probe of the cosmological density field at early epochs.

In this paper we start investigating the above issue by collecting all the available data for one of these candidate filaments, and supplementing it with our own observations with the MAMBO array at the focus of the IRAM 30m antenna at 1.2mm.

The addition of mm data is crucial in constraining the nature of the obscured $24\mu\text{m}$ sources. In fact their nature is currently under debate: a large fraction of them has radio spectral indices typical of *frustrated* radio-loud Active Galactic Nuclei (AGNs) (Magliocchetti et al. 2008a) but their q values – i.e. the values of the ratio between far-IR (FIR) and radio flux densities – are similar to those of star forming objects (i.e. Ibar et al. 2008). Their colours indicate mixed AGN and starburst properties (Magliocchetti et al. 2007; Pope et al. 2008; Lonsdale et al. 2009).

FIR/mm observations are very effective for determining the bolometric output by measuring the redshifted peak of the dust emission, for characterizing the broad band spectrum which allows to separate AGN from starburst emissions, and for studying the parallel dust obscured evolution of super-massive BHs (SMBHs) and of their host galaxies. The AGN contribution produces hotter dust and much higher $F(\text{mid-IR})/F(\text{sub-mm})$ ratios than (sub)mm selected sources, which are generally high- z starburst galaxies. Lutz et al. (2005) found a mean ratio $F_{1.2\text{mm}}/F_{24\mu\text{m}} = 0.15 \pm 0.03$ for a sample of AGN-dominated optically obscured Spitzer FLS sources with $F_{24\mu\text{m}} > 1\text{mJy}$. Spitzer observations of starburst-dominated objects originally detected with SCUBA and MAMBO (Pope et al., 2006, Ivison et al.,

2007, Lonsdale et al., 2008) and with $F_{24\mu\text{m}} > 20\text{mJy}$, instead have a median $F_{850\mu\text{m}}/F_{24\mu\text{m}} \simeq 25$ and $F_{1.2\text{mm}}/F_{24\mu\text{m}} \simeq 12$.

Estimating the AGN and star-forming components helps in investigating any evolutionary connection between them, as the relationship between the star-formation history and the growth of the active nucleus is a key ingredient for understanding the physics of the evolution of both massive galaxies and AGNs (Granato et al. 2004; Schawinski et al. 2006).

This work deals with a candidate protocluster system of optically obscured $24\mu\text{m}$ Spitzer FLS sources in the field of an extended radio-loud AGN. Such a system: i) provides us with a sample of sources with a $24\mu\text{m}$ flux distribution which is representative of that found for the whole (Magliocchetti et al. 2007) dataset; ii) allows us to investigate in a direct way the transition between 'pure' star-forming galaxies and AGN-dominated sources as envisaged e.g. by the Granato et al. model; iii) perhaps most importantly, it provides an excellent laboratory to study the large-scale interplay between AGN activity (such as that produced by radio jets) and star formation in the sources belonging to the protocluster.

The central source of this complex radio system is identified with FLSVLA172010.2+592425.2 (Condon et al. 2003) and at $8''$ from it there is another radio source, 7C1719+5927 (Hales et al 1995). The flux densities integrated over the whole system at 38, 330, 610 MHz, and 1.4GHz are of 2000, 143, 33.7, and 35.6 mJy, respectively. The 38, 330, and 1.4 GHz measurements are consistent with a power-law spectrum ($S \propto \nu^{-\alpha}$, with $\alpha \simeq 1$), while the 610 MHz flux density is a factor $\simeq 2$ below that. The central source has an optical counterpart with a magnitude of $R = 23.67$ (Fadda et al. 2004). The spectroscopic redshift of this source is unknown.

Section 2 reports all the data available on this sample and the new MAMBO observations. Results of our analysis are given in §3 and discussed in §4, while in §5 we summarize our main conclusions.

2 DATA

The source sample used in this work was drawn from a parent sample whose selection criteria are outlined in this section.

2.1 Sample selection and Spitzer data

Of the original 793 $R > 25.5$ sources in the Magliocchetti et al. (2007) sample, 510 have IRAC photometry. On the basis of these data, sources were classified according to their $F_{8\mu\text{m}}/F_{24\mu\text{m}}$ and $F_{4.5\mu\text{m}}/F_{3.6\mu\text{m}}$ colours (Magliocchetti et al. 2008a) as follows:

- AGN0: $F_{24\mu\text{m}} \geq 0.6\text{mJy}$; $F_{8\mu\text{m}}/F_{24\mu\text{m}} \geq 0.1$;
- SB0 (starburst): $F_{24\mu\text{m}} \geq 0.6\text{mJy}$; $F_{8\mu\text{m}}/F_{24\mu\text{m}} < 0.1$;
- AGN1: $F_{24\mu\text{m}} < 0.6\text{mJy}$; $F_{4.5\mu\text{m}}/F_{3.6\mu\text{m}} \geq 4.5/3.6$;
- Unclassified: $F_{24\mu\text{m}} < 0.6\text{mJy}$; $F_{4.5\mu\text{m}}/F_{3.6\mu\text{m}} < 4.5/3.6$ or no IRAC information.

The above classification is consistent with the results of mid-infrared (IRS) spectroscopy of samples of heavily obscured

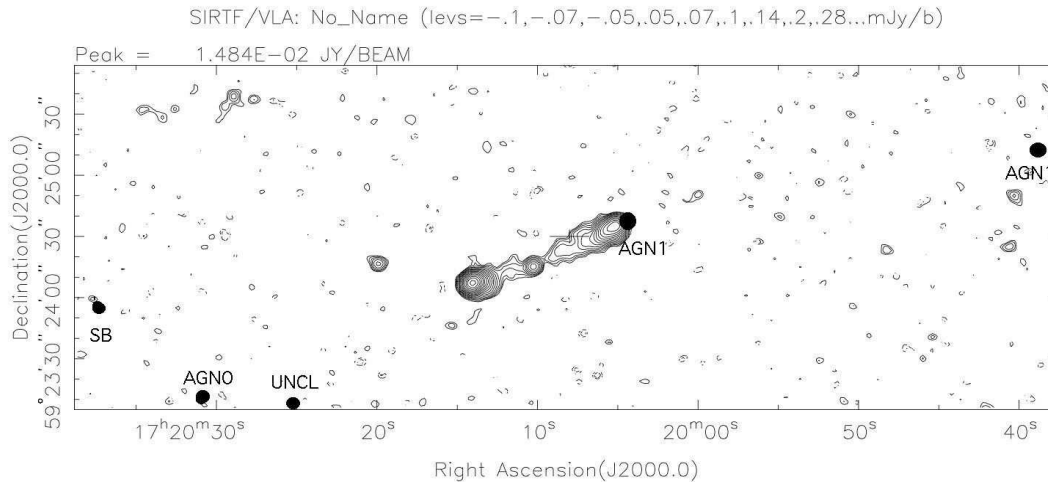


Figure 1. *Spitzer*/VLA field centered at 17:20:05, +59:24:30. Filled circles correspond to the FLS *Spitzer* 24 μ m sources we observed with MAMBO.

24 μ m-bright objects (brighter than ~ 0.7 –1 mJy). The majority of them have spectral shapes indicative of a buried AGN (Martinez-Sansigre et al. 2006; Yan et al. 2005, 2007; Brand et al. 2007; Weedman et al. 2006a,b; Pope et al. 2008).

2.2 Radio observations: selection of protoclusters

Magliocchetti et al. (2008a) searched for radio counterparts to optically obscured *Spitzer* sources by cross-correlating the source sample of Magliocchetti et al. (2007) with the radio source catalogs by Condon et al. (2003) at 1.4GHz, Morganti et al. (2004) at 1.4GHz and Garn et al. (2007) at 610 MHz.

A number of the selected sources turned out to lie in overdense regions of the sky in the neighborhood of radio-loud AGNs (see, e.g., Fig. 1). To pursue our research further we then selected small complete subsamples in those high density regions with deep radio imaging and hosting a radio-loud AGN. In this paper we concentrate on the field shown in Fig. 1. The available *Spitzer*, radio and optical photometric data are listed in Table 1.

2.3 Redshift constraints: IRAC and optical observations

IRAC photometry can also be used to provide rough redshift estimates for those sources whose SEDs present a contribu-

tion from an evolved stellar population in the 3.6 μ m and 4.5 μ m bands. Based on the form of the SED in this wavelength range (see Fig. 6 in Magliocchetti et al. 2008a), and in particular on its interpolated slope β ($F \propto \lambda^\beta$) between 3.6 μ m and 4.5 μ m, we estimated that the redshifts of these objects are around $z \sim 1.7$. This makes it plausible that they are physically associated and not just close to one another due to projection effects.

An independent assessment of the redshift range for this source population comes from the measured spectroscopic redshifts of optically faint 24 μ m *Spitzer* sources by Dey et al. (2008) using the IRS *Spitzer* spectrograph and Keck optical spectroscopy. If we adopt Dey et al.’s colour criterion, our sources have a median redshift $\langle z \rangle = 1.8$ –1.9, roughly consistent with our previous estimate.

2.4 MAMBO observations of the candidate protocluster

Data were taken with the 117-channel Max Planck Millimetre Bolometer Array (MAMBO; Kreysa et al. 1998) at the focus of the 30m IRAM antenna at Pico Veleta. Chopping photometry at 2Hz with 32'' throw in azimuth was gathered at 250 GHz (1.25 mm) in observing pool during Winter 2008 towards the sources listed in Tables 1 and 2. Data were obtained in good observing conditions (250 GHz atmo-

Source name	R_{mag}	$3.6\mu\text{m}$ μJy	$4.5\mu\text{m}$ μJy	$5.8\mu\text{m}$ μJy	$8\mu\text{m}$ μJy	$24\mu\text{m}$ μJy	1.4GHz μJy	610MHz μJy	ID
J172037.75+592359.3	>25.5	29.93±4.33	45.84±6.24	<100	<100	400±80	<100	<182	SB
J172030.92+592308.3	>25.5	64.68±7.84	53.51±7.15	<100	191.4±24.3	390±75	<100	<182	AGN0
J172005.01+592430.0	>25.5	24.36±3.65	33.52±5.18	<100	<100	440±88	–	–	AGN1
J171939.17+592512.4	>25.5	20.89±3.37	36.59±5.44	<100	<100	380±74	157±27	<182	AGN1
J172025.20+592308.0	>25.5	<100	<100	<100	<100	350±70	<100	<182	UNCL

Table 1. Optically obscured $24\mu\text{m}$ *Spitzer* sources observed with MAMBO during Winter 2008. The table lists the optical and *Spitzer* photometry available for these sources. Last two columns report the radio measurements when available. The source J172005+592430 lies on top of a lobe of the radio source (see Fig. 1), that hides its possible radio emission. Upper limits are at the 3σ level. The last column shows the type of identification assigned by Magliocchetti et al. (2007) to these sources. We have assigned in our analysis an error-bar of 20% to the $24\mu\text{m}$ fluxes (cfr text).

Source name	weighted flux (mJy)	first observation (mJy)	atmospheric transmission τ	average atm noise (mJys ^{1/2})	on source int time (min)	second observation (mJy)	atmospheric transmission τ	average atm noise (mJys ^{1/2})	on source int time (min)
J172037.75+592359.3	1.4±0.5	1.2±0.5	0.35	36	160	3.4±1.4	0.15	90	52
J172030.92+592308.3	<1.2	0.12±0.63	0.16	50	48	-0.13±0.58	0.36	40	64
J172005.01+592430.0	1.6±0.3	1.0±0.5	0.37	46	80	2.2±0.5	0.27	63	72
J171939.17+592512.4	1.4±0.5	1.3±0.6	0.5	90	102	1.3±0.6	0.3	40	52
J172025.20+592308.0	1.8±0.4 [†]	0.7±0.6	0.35	40	60	2.5±0.6	0.26	60	80

Table 2. MAMBO observations of $24\mu\text{m}$ optically obscured *Spitzer* sources. The sources observed were previously classified – according to our colour selection criterion (Magliocchetti et al., 2007) – as either starbursts or obscured AGNs. The only undetected source was indeed classified as an AGN and its flux upper limit is 1.2 mJy (3σ). Atmospheric values in columns 4,5,8,9 refer to average values during the observations. Errors on the fluxes are statistical. Final flux is computed as a weighted average.

[†] Because of the discrepancy between the two measurements of this source, we assign in our analysis an additional systematic error-bar of 20% to its mm flux.

spheric opacity better than 0.2 and low sky noise), as resulting from the regular checks of atmospheric transmission and noise. Pointing was checked every hour with a nearby quasar. Each source has been observed in at least two independent runs. Data were reduced with the MOPSIC software (Zylka 1998).

To check for any malfunctioning of the detecting system with consequent instabilities of the bolometer output, we inspected subscan by subscan and reduced the data separately for each observing chunk. Subscans containing spikes (less than 10% of the total) were discarded. Observing logs with total integration times on sources, atmospheric parameters, fluxes at each run and the final calibrated fluxes with statistical errorbars are reported in Table 2. Longer integration times were necessary because of the higher sky noise during some of the observations. Statistically, the sky noise was behaving properly as it scales with the square root of the integration time.

3 RESULTS

3.1 Interpreting the observed spectral energy distributions

Figure 2 shows the photometric points from the R magnitude down to the radio fluxes at 1.4 GHz and 610 MHz for the sources of our sample. This also includes the MAMBO observations presented in Section 2.4. The original $24\mu\text{m}$ errorbars given by Fadda et al (2006) for these sources are unrealistically small (1.5%); on the suggestion by the referee, we have adopted 20% error bars, as estimated for similar (80s) integration times.

In Table 3 we report the results from two different types of fits and the corresponding χ^2 values and luminosities. The first template used is the Arp220 SED, while the second has two components: Arp220 SED and an obscured torus template made available by Polletta et al. (2007). In this latter case we could estimate the contribution to the bolometric luminosity of the two components. We find that the Arp 220 Spectral Energy Distribution (SED) provides the best single component fit for all the observed SEDs. In fact, all of the 30 SEDs of nearby star-forming galaxies presented by Vega

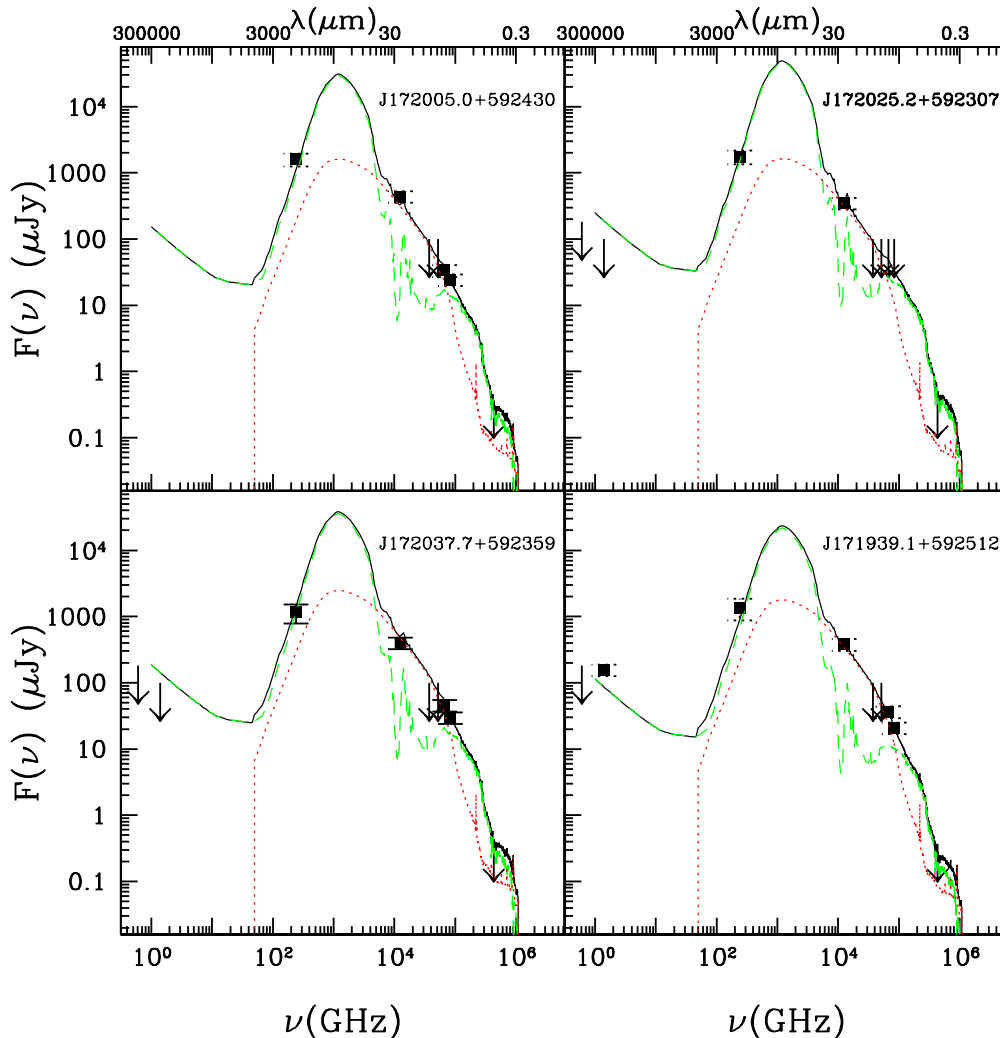


Figure 2. Spectral energy distributions of the four sources detected with MAMBO in our sample. Photometric points from the R magnitude down to the radio fluxes at 1.4 GHz and the 610 MHz are shown together with two spectral energy distributions which best fit the observed points: a starburst component represented by Arp220 SED (green dashed line) and an obscured torus (Polletta et al., 2007, red dotted line). The SEDs are shifted to a redshift of 1.73. The corresponding bolometric luminosities are $5\text{--}7 \times 10^{12} L_{\odot}$ (see Table 3).

et al. (2008) and the other template SEDs made available by Polletta (Polletta et al. 2007) give substantially worse fits. By then using the Arp 220 SED as ‘bona fide’ template, we get a minimum χ^2 fit at the same value of the redshift, $z = 1.73$, for each object belonging to the filament separately, with the exception of J172030.9+592310 which is classified as an AGN0 from IRAC photometry (see Table 1). At this redshift, the sources have bolometric luminosities in the range $5\text{--}7 \cdot 10^{12} L_{\odot}$ and star formation rates of $\sim 1000 M_{\odot}/\text{yr}$ (see Table 3)². Obviously, this surmise can only be confirmed by spectroscopic redshift measurements.

No really good fit could be found for J172030.9+592310. In this case, neither the Arp 220 template, nor any other template mentioned above, can be accepted as a realistic de-

scription of its SED. The lowest χ^2 , still quite unsatisfactory ($\chi^2 = 23.9$), fit was obtained by adding to the SED of Arp 220 the Polletta’s ‘torus’ template (heavily obscured AGN) at $z = 1.214$ (green line in Fig. 3). Additionally, Figure 3 shows as a red line the best-fit with the same combination of SEDs red-shifted to $z = 1.73$. This shift in z substantially worsens the χ^2 value ($\chi^2 = 48.5$).

In Table 3 we give the estimated bolometric luminosities of the sources for the two models we have considered, i.e. pure starburst SED (I fit) and starburst plus AGN (II fit). The errors on the total luminosities were computed finding the contours in the parameter space for which $\chi^2 = \chi^2_{\min} + 1$ and computing the maximum and minimum luminosities on these contours. The resulting errors are of 30–35%. The main contribution to them comes from the uncertainties on redshifts of the sources, which turn out to be $\Delta z \simeq 0.17\text{--}0.20$. In the case of the SB+AGN fit we give the estimated bolometric luminosities of each component. The global bolometric

² The star formation rate was estimated from the total far-IR luminosity, which is essentially equal to the bolometric luminosity, using eq. (4) of Kennicutt (1998).

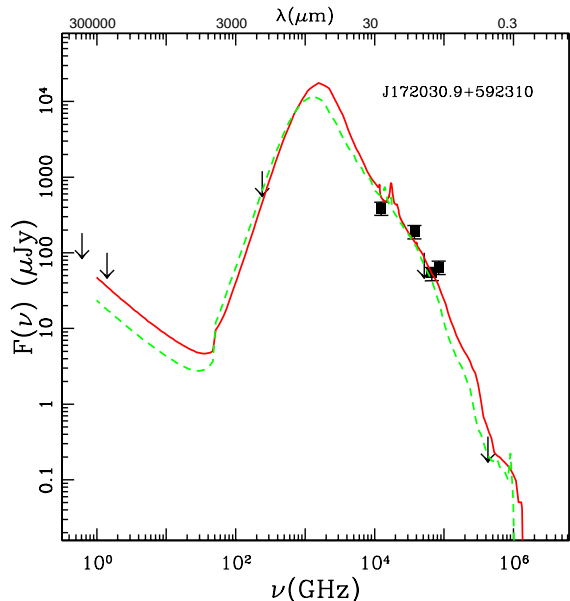


Figure 3. Spectral energy distribution as in Figure 2 for the AGN0. The green dashed line shows the best fit, obtained adding the SED of Arp 220 with Polletta’s “obscured torus” template, red-shifted to $z = 1.214$; the red solid line shows the best-fit (giving a much worse χ^2) derived with the same combination of SEDs red-shifted to $z = 1.73$. We classify this source as a type 2 AGN candidate, i.e. an obscured AGN.

luminosity is therefore the sum of the two contributions, and it is used to compute, in a consistent way, the SB and AGN fractions. The estimate of the bolometric luminosity clearly depends on the used SED template. No surprise that 2 substantially different templates yield different results. Note, however, that differences are not very large. In the worst case (source J171939.1, leaving aside the pathological second source), going from a pure Arp220 template to a SB+AGN template decreases the bolometric luminosity by 36%. We do not attach any profound implication to the fact that for 3 sources the bolometric luminosity decreases from case I to case II, while only in one case (last source) it increases: this is most likely happening by chance.

Based on the SED analysis which is listed in Table 3, we find that the nature of our candidate protocluster members can be summarized as follows: the AGN contribution to the bolometric luminosities ranges between 14 and 26% of the total. A $\simeq 14\%$ contribution to the total bolometric luminosity is enough for the AGN to dominate the emission at 5.8, 8 and $24\mu\text{m}$, while the SB dominates at 1.25mm and at $\lambda < 4.5\mu\text{m}$. The above fits are consistent with all these sources being at the same redshift.

3.2 Nature of the obscured *Spitzer* $24\mu\text{m}$ sources

The information provided by the spectral energy distribution is not, however, compelling and the nature of these sources cannot be entirely evinced. However colour–colour plots may be further exploited to support our previous findings on the origin of the source emission. We compare in this section the colours of the sources presented in this work with those of other $24\mu\text{m}$ *Spitzer* sources, extracted with

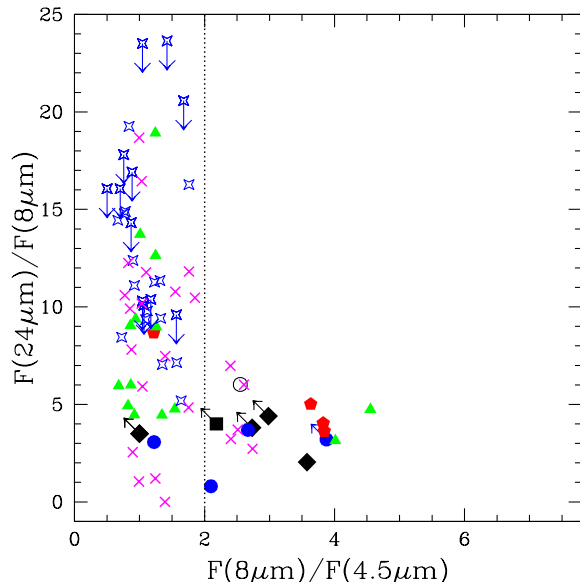


Figure 4. The colour–colour $F(24\mu\text{m})/F(8\mu\text{m})$ vs. $F(8\mu\text{m})/F(4.5\mu\text{m})$ plot is used as a diagnostic tool to discriminate between starburst and AGN dominated SEDs. The vertical dashed line corresponds to the ratio $F(8\mu\text{m})/F(4.5\mu\text{m}) = 2$, proposed by Pope et al. (2008) as the boundary between SB (having ratios < 2) and AGN dominated SEDs. Filled squares correspond to the *Spitzer* sources presented in this work (we note that for all but one case the $8\mu\text{m}$ measurement is a mere upper limit); filled triangles: Ivison et al. (2004); filled pentagon: Younger et al. (2007); filled circles: Sawicki & Webb (2005); crosses: Pope et al. (2006); four-points stars: Lonsdale et al. (2008).

different colour criteria, and with those of the SMGs, in the effort to elucidate the nature of the objects belonging to our candidate protocluster.

3.2.1 Colour–colour diagrammes

In the original paper by Magliocchetti et al. (2007) the distribution of the $F_{8\mu\text{m}}/F_{24\mu\text{m}}$ versus the $F_{\text{R}}/F_{24\mu\text{m}}$ colours has been shown as a powerful tool to discriminate between starburst dominated ($F_{8\mu\text{m}}/F_{24\mu\text{m}} < 1$) from AGN dominated ($F_{8\mu\text{m}}/F_{24\mu\text{m}} > 1$) objects among the optical obscured $24\mu\text{m}$ sources (see their Figure 2). The SED fitting results obtained in section 3.1 for all sources but J172030.9+592310 are consistent with the preliminary estimates obtained from the location of such sources in the $[\nu_{24}F(24\mu\text{m})/\nu_{\text{R}}F_{\text{R}}, \nu_{24}F(24\mu\text{m})/\nu_{8}F(8\mu\text{m})]$ colour–colour plane. Sources of this sample have $\log(\nu_{24}F(24\mu\text{m})/(\nu_{\text{R}}F_{\text{R}})) > 1.74$ and $\log(\nu_{24}F(24\mu\text{m})/\nu_{8}F(8\mu\text{m})) > 0.55$, corresponding to the colours of NGC 4418 (heavily obscured galaxy) shifted to a redshift of 2 (Lutz et al. 2005), with the only exception of the AGN0 which has $\log(\nu_{24}F(24\mu\text{m})/\nu_{8}F(8\mu\text{m})) = 0.3$ and $\log(\nu_{24}F(24\mu\text{m})/(\nu_{\text{R}}F_{\text{R}})) > 1.74$, putting it closer to the expected colours of the NGC1068 nucleus at a redshift around 2.

The values of the 1.2mm/ $24\mu\text{m}$ flux ratios which are higher for the sources of the *Spitzer* sample of this work range from 3 to 5, except for the AGN0, which has $F(1.2\text{mm})/F(24\mu\text{m}) < 3$. On a $F(24\mu\text{m})$ versus redshift plot these values coincide with those obtained by Lonsdale

Source name	χ^2 I fit (5 d.o.f.)	L_{bol} I fit L_{\odot}	χ^2 II fit (4 d.o.f.)	L_{SB} II fit L_{\odot}	L_{AGN} II fit L_{\odot}
J172037.7+592359	6.6	6.5×10^{12}	0.23	4.1×10^{12}	1.2×10^{12}
J172030.9+592310	81	7.1×10^{12}	23.9	1.0×10^{12}	0.5×10^{12}
J172005.0+592430	2.4	5.7×10^{12}	2.4	3.4×10^{12}	0.8×10^{12}
J171939.1+592512	4.6	5.3×10^{12}	1.4	2.5×10^{12}	0.9×10^{12}
J172025.2+592307	2.5	5.2×10^{12}	1.1	5.5×10^{12}	0.8×10^{12}

Table 3. Results of the minimum χ^2 fits. Fit I is obtained adopting the Arp 220 SED (columns 2 and 3). Adding an obscured AGN component (fit II, columns 4-6) improves the χ^2 values for three of the sources (we leave aside the source J172030.9+592310 for which no acceptable fit was obtained; see text). We note that these results are only indicative as the number of photometric points is too small to allow any firm conclusion. The errorbars of the $24\mu\text{m}$ fluxes have been set to 20%. Errorbars on the total luminosities are estimated to be 30% - 35% (see text for detail).

et al. (2008) for SWIRE sources (see their Fig. 8). Lonsdale et al. (2008) have observed a large part of the SWIRE sample at 1.2mm with the MAMBO array and have shown that the SWIRE sources and sub-mm selected galaxies (SMGs) have similar mm fluxes, but the latter have $F(1.2\text{mm})/F(24\mu\text{m})$ ratios higher than the former by a factor of 2 to 10. *Spitzer* optically obscured sources have values intermediate between those of the SMGs and those characteristic of AGNs. This finding is independently confirmed by IRS spectra of SWIRE sources which show that part of the $24\mu\text{m}$ flux is due to a hidden AGN.

In Fig. 4 the location in the $[F(24\mu\text{m})/F(8\mu\text{m}), F(8\mu\text{m})/F(4.5\mu\text{m})]$ plane of our four sources with IRAC fluxes are compared with those of the SMGs and of the dust obscured galaxies (DOGs; Pope et al. 2008). This colour-colour diagram was used by Ivison et al. (2004) as a diagnostic tool to discriminate between starburst (SB) dominated and AGN dominated SMGs detected by *Spitzer*. Their SMGs turned out to lie in the locus of SB dominated galaxies, except for two with AGN colours. The same diagram was used by Pope et al. (2008) to classify their DOGs ($R - [24] > 14$ and $F(24\mu\text{m}) > 100 \mu\text{Jy}$). These authors proposed the ratio $F(8\mu\text{m})/F(4.5\mu\text{m}) = 2$ as the boundary between SB (lower values of the ratio) and AGN dominated SEDs. The conclusion was that 80% of the DOGs are starburst dominated.

All the sources analysed in this work but one (cfr Table 1 and Figures 2, 3) have $8\mu\text{m}$ fluxes below the sensitivity threshold of the relevant IRAC channel (i.e. $100 \mu\text{Jy}$), yielding upper limits to the $8\mu\text{m}/4.5\mu\text{m}$ ratio in the range 2.2-3, and lower limits to the $24\mu\text{m}/8\mu\text{m}$ ratio in the range 3.8-4.4. For the measured $24\mu\text{m}$ fluxes, this is indicative of a star-forming SED as an AGN/power-law SED most likely would have implied detectable $8\mu\text{m}$ fluxes. In addition, adopting the Pope et al.'s (2008) criterion, our sources may have a SB component, though the $8\mu\text{m}$ observations are not deep enough to certain. The only exception is J172030.9+592310 which has $8\mu\text{m}/4.5\mu\text{m} \simeq 3.6$ and is therefore clearly in the realm of AGNs.

IRAC photometry helps further in diagnosing the nature of these sources. In particular the $[8\mu\text{m}/4.5\mu\text{m}, 5.8\mu\text{m}/3.6\mu\text{m}]$ colours can be used to distinguish SEDs with evolved stellar population (which would determine

a 'bump' in the SED between 3 and $8\mu\text{m}$ in the observed frame) and those with a power-law continuum all through the IRAC channels, characteristic of AGNs (i.e. Magliocchetti et al., 2008a and Yun et al. 2008). Although we cannot draw any strong conclusion because of the lack of accurate IRAC photometry, we have at least upper limits on the flux ratios for the four sources detected by MAMBO, in the ranges $\log F(8\mu\text{m})/F(4.5\mu\text{m}) \leq 0.3-0.5$ and $\log F(5.8\mu\text{m})/F(3.6\mu\text{m}) \leq 0.5-0.7$, while the AGN0 has $\log F(8\mu\text{m})/F(4.5\mu\text{m}) = 0.55$ and $\log F(5.8\mu\text{m})/F(3.6\mu\text{m}) \leq 0.2$. The diagnostic diagrams of Yun et al. (2008) then confirm the conclusions above, i.e. the sources studied in this work are dominated by star formation (SF) processes and have similar properties to the DOGs (Pope et al. 2008).

As we have just seen, *Spitzer* data give strong hints on the nature of our sources. However, they do not allow us to unambiguously characterize them as they cannot provide direct information on their relationship with SMGs and on the importance of the AGN contribution to their SEDs. We can then go a step forward and exploit further information. For example, by using the mm and radio fluxes, together with the upper limits, we investigate the well-known, tight relationship between radio and far-IR emissions. The origin of this relation is attributed to star formation processes and has been extensively investigated for a quarter of a century. It is firmly established for the local Universe (i.e. Helou, Soifer, Rowan-Robinson 1985) and appears to also extend to higher redshifts (e.g. Garrett 2002; Appleton et al. 2004; Ibar et al. 2008; Garn & Alexander 2009).

By then comparing the $[850\mu\text{m}/1.4\text{GHz}, 850\mu\text{m}/24\mu\text{m}]$ colours of the *Spitzer* obscured sources with those SMGs having a radio and *Spitzer* counterpart we find that the latter have lower $850\mu\text{m}/1.4\text{GHz}$ and $850\mu\text{m}/24\mu\text{m}$ ratios but both follow very tightly the correlation between the two colours, indicating once again that the sources in our sample with measured MAMBO fluxes are dominated by SF processes.

The above correlation can also be exploited to estimate the redshift from the $F(850\mu\text{m})/F(1.4\text{GHz})$ ratio, using the Carilli & Yun (1999) plot. We convert the MAMBO 1.2 mm fluxes to $850\mu\text{m}$ fluxes using the median ratio

$F_{850\mu\text{m}}/F_{1.2\text{mm}} \simeq 2.5$, as found by Greve et al. (2004), for SCUBA galaxies at $z \sim 2$. The source with 1.4 GHz radio flux has $850\mu\text{m}/1.4\text{GHz} \simeq 22$, placing it in the redshift interval 1–2.2. The 2 sources with radio upper limits have $850\mu\text{m}/1.4\text{GHz} > 30$ and > 45 and redshifts > 1.3 and > 1.5 , respectively.

As for the Spitzer source coinciding with the radio lobe, the convolution of the radio map with a Gaussian of FWHM corresponding to the $24\mu\text{m}$ MIPS beam ($6''$) gives a flux at 1.4 GHz of ~ 3 mJy. The MIPS beam is comparable to the resolution of the radio VLA 1.4 GHz observations, which was $5''$.

This value could be entirely associated to the lobe itself or may be due to the overlap of two components: one associated to the $24\mu\text{m}$ source and one to the lobe. We therefore consider this value as an upper limit to the real radio emission of this Spitzer source. In any case the correlation FIR-radio, which is the underlying assumption to infer the redshift, cannot be applied.

4 DISCUSSION

As is widely known, the flux of sources at a redshift around 2 in the *Spitzer* $24\mu\text{m}$ channel may contain emission from the PAH feature at a rest frame wavelength of $7.7\mu\text{m}$. Since this feature is associated to star forming processes, the sample selection based on the $24\mu\text{m}$ flux is biased as it enhances the probability of detecting star forming sources at this epoch.

This flux band has been extensively used to estimate star formation in galaxies (see, e.g., Calzetti 2008 for a recent review and Rieke et al. 2009 for local galaxies). However, the use of this band alone requires many *a priori* assumptions (e.g. comparison with low-redshift SEDs, PAH evolution, metallicity and the conditions in the photon dissociation regions) on the overall spectral energy distribution and completely misses star formation processes associated to molecular gas. We have estimated the star formation rate by fitting all the available photometric data on these sources. It follows that the uncertainties in this case are more related to the unavailability of the far-infrared fluxes, which can only be retrieved with future Herschel observations, and to the scant knowledge of the AGN contribution in the mid-IR domain. Because of their optical faintness ($R > 25.5$) spectroscopic redshifts of these objects are hard to obtain and they will be ideal candidates for ALMA follow-up observations.

Given the above difficulties, we tried to infer the nature of the sources in our sample from colour–colour plots, coming to the conclusion that the *Spitzer* optically obscured sources belonging to the analysed protocluster are likely to host an AGN and their mid-IR fluxes may be affected by its emission. Quantifying this effect will be only possible when far-IR observations will allow us to derive the starburst contribution to the SEDs.

One of the sources studied in this work has its position coinciding with one of the radio lobes of the radio loud AGN. At the locations of the radio core and of the second radio lobe there are no *Spitzer* detected sources. The convolution of the radio flux coinciding with the location of the *Spitzer*

source gives a flux at 1.4GHz of ~ 3 mJy, which we consider as an upper limit to its real radio emission.

The central source of this complex radio system is identified with FLSVLA172010.2+592425.2 (Condon et al. 2003) and at $8''$ from it there is another radio source, 7C1719+5927 (Hales et al 1995). The flux densities integrated over the whole system at 38, 330, 610 MHz, and 1.4GHz are of 2000, 143, 33.7, and 35.6 mJy, respectively. The 38, 330, and 1.4 GHz measurements are consistent with a power-law spectrum ($S \propto \nu^{-\alpha}$, with $\alpha \simeq 1$), while the 610 MHz flux density is a factor $\simeq 2$ below that. This atypical behaviour deserves further investigation. The central source has an optical counterpart with a magnitude of $R = 23.67$ (Fadda et al. 2004). The optical redshift of this source is unknown. Using the R magnitude-redshift relationship for radio sources given by Rigby, Snellen, & Best [2007; their eqs. (9) and (10)] we find $z \sim 1.55$. Within the rather large uncertainties associated to this relationship, especially at $z \gtrsim 1$ (see Fig. 6 of Rigby et al. 2007), this estimate is compatible with the radio source being at the estimated redshift of our *Spitzer* sources. If located at $z = 1.73$, the total luminosity at 1.4 GHz for the “concordance” cosmology (spatially flat universe with $\Omega_\Lambda = 0.7$ and $H_0 = 70 \text{ km s}^{-1} \text{ Mpc}^{-1}$), and a spectral index $\alpha = 1$, is $7 \cdot 10^{33} \text{ erg s}^{-1} \text{ Hz}^{-1}$, i.e. a luminosity which is typical of an FR II (Fanaroff & Riley 1974) radio galaxy, consistent with its edge-brightened morphology.

The total number of radio sources in the VLA-FLS area, as obtained by Condon et al (2003), brighter than 30 mJy is 18. We then set, following Brookes et al. (2008), the fraction of radio sources at $z > 2$ to be about 10%. By doing this we expect about 2 extended radio sources in the VLA-FLS field brighter than 30 mJy and with $z > 2$. This number coincides with the two examples of extended radio sources associated to overdensities of Spitzer-obscured galaxies in the FLS (the other case is currently under study). We can then conclude that, despite of the small statistics there is a possible association of extended radio sources at $z \sim 2$ with active mid-IR galaxies.

5 CONCLUSIONS

To test the possibility that the selected sources belong to a candidate protocluster and shed light on the nature of optically obscured galaxies defining the candidate filaments, we have carried out observations with the MAMBO array at the IRAM 30m antenna on Pico Veleta of five optically obscured sources. These latter trace one of the best examples of a candidate filament, centered on a radio galaxy and roughly aligned with its jets. One of the *Spitzer* sources is located right at the edge of one of its radio lobes. Four of the observed sources were detected. Although the available data are insufficient to draw firm conclusions, the SEDs, obtained by combining our measurements with optical, infrared and radio observations, are consistent with the 4 detected sources being at the same $z \simeq 1.73$ redshift and, therefore, tracing a real filament with a physical size of $\simeq 4 \text{ Mpc}$, which may evolve into a rich galaxy cluster centered on a powerful radio-galaxy.

The 4 detected sources most likely lie in the region of the $[24\mu\text{m}/8\mu\text{m}, 8\mu\text{m}/4.5\mu\text{m}]$ colour-colour plot occupied

by dust obscured galaxies (DOGs; Pope et al. 2008). The Arp220 SED provides reasonably acceptable fits for them. At the estimated redshift, the fits imply bolometric luminosities in the range $5\text{--}7 \cdot 10^{12} L_{\odot}$ and star formation rates of $\sim 1000 M_{\odot}/\text{yr}$. Their IR colours, however, are bluer than those of sub-mm bright galaxies, suggesting either a significant AGN contribution to IRAC fluxes or the presence of warmer dust, perhaps heated by young starbursts. In fact, adding an obscured AGN component improves the χ^2 values for three of the 4 sources. The best fit AGN contributions to the bolometric luminosities range from 14 to 26% of the total. This is enough for the AGN to dominate the emission at 5.8, 8 and $24\mu\text{m}$, while the SB dominates at 1.25mm and at $\lambda < 4.5\mu\text{m}$. The new fits are again consistent with all these sources being at the same redshift, $\simeq 1.73$.

The source J172030.9+592310 may be a foreground object at $z \simeq 1.2$, although the redshift estimate is very uncertain. Its SED is best interpreted as the combination of that of Arp220 with the “torus template”, corresponding to the model used to fit the SED of a heavily obscured type 2 QSO, SWIRE J104409.95+585224.8 (Polletta et al. 2006). At $z \simeq 1.2$, the best fit luminosities of the starburst and of the AGN components are $1.0 \times 10^{12} L_{\odot}$ and $0.55 \times 10^{12} L_{\odot}$, respectively.

A large-scale interplay between AGN activity (such as that produced by radio jets) and star formation in the sources belonging to the protocluster may be at work here and may shape the properties of these sources. Following West (1994) we suggest that the protocluster may be in the process of forming the dominant cluster galaxy from the central powerful radio galaxy. To substantiate this rather speculative interpretation we are extending this investigation to other similar fields.

6 ACKNOWLEDGEMENTS

This work is based in part on observations taken with the IRAM 30m antenna, IRAM is supported by INSU/CNRS (France), MPG (Germany) and IGN (Spain). We are grateful to the IRAM staff at Pico Veleta and in particular to Stephan Leon for his assistance with the pool observations. We also thank A. Bressan for having made available the galaxy templates of Vega et al. (2008) in tabular form. GDZ acknowledges partial financial support from ASI contracts I/016/07/0 “COFIS” and “Planck LFI Activity of Phase E2”. The authors wish to thank the referee for her/his suggestions that helped in improving the paper.

REFERENCES

- Appleton P.N., et al., 2004, ApJ Supplement 154, 147
 Brand K., et al., 2007, ApJ 663, 204
 Brodwin M., et al., 2008, ApJ, 687, L65
 Brookes M. H., Best P. N., Peacock J. A., Röttgering H. J. A., Dunlop J. S., 2008, MNRAS, 385, 1297
 Calzetti D., 2008, ASPC, 390, 121
 Carilli C.L., Yun M.S., 1999, ApJ 513, L13
 Charmandaris V., et al., 2004, ApJ Supplement 154, 142
 Condon J.J., Cotton W.D., Yin Q.F., Shupe D.L., Storrie-Lombardi L.J., Helou G., Soifer B.T., Werner M.W., 2003, AJ, 125, 2411
 Dannerbauer H., Walter F., Morrison G., 2008, ApJ 673, L127
 Desai V., et al., 2007 ApJ 669, 810
 Dey A., et al., 2008, ApJ 677, 943
 Egami E., et al., 2004, ApJS 154, 130
 Fadda D., Jannuzi B.T., Ford A., Storrie-Lombardi L.J., 2004, AJ, 128, 1
 Fadda D. et al., 2006, AJ, 131, 2859
 Fanaroff B. L., Riley J. M., 1974, MNRAS, 167, 31P
 Farrah D., et al., 2006, ApJ 641, L17
 Garn T., Green D.A., Hales S.E.G., Riley J.M., Alexander P., 2007, MNRAS, 376, 1251
 Garn T., Alexander P., 2008, MNRAS 394, 105
 Garrett M.A. 2002, A&A 384, L19
 Granato G.L., De Zotti G., Silva L., Bressan A., Danese L., 2004, ApJ, 600, 580
 Greve T. R., Ivison R. J., Bertoldi F., Stevens J. A., Dunlop J. S., Lutz D., Carilli C. L., 2004, MNRAS, 354, 779
 Hales S.E.G., Waldrum E.M., Rees N., Warner P.J., 1995, MNRAS 274, 447
 Helou G., Soifer B. T., Rowan-Robinson M., 1985, ApJ, 298, L7
 Houck J. R., et al., 2005, ApJ, 622, L105
 Ibar E., et al., 2008, MNRAS 386, 953
 Ivison R.J., et al., 2004, ApJ Supplement 154, 124
 Ivison R.J., et al., 2007, MNRAS 380, 199
 Kennicutt R. 1998, ARAA 36, 189
 Kreysa E., et al., 1998, SPIE vol. 3357, 319-325
 Lonsdale C., et al., 2009, ApJ 692, 422
 Lutz D., Yan L., Armus L., Helou G., Tacconi L.J., Genzel R., Baker A.J., 2005, ApJ 632, L13
 Magliocchetti M., Silva L., Lapi A., De Zotti G., Granato G.L., Fadda D., Danese L., 2007, MNRAS, 375, 1121
 Magliocchetti M., Andreani P., Zwaan M., 2008a, MNRAS 383, 479
 Magliocchetti M., et al., 2008, MNRAS, 383, 1131
 Martinez-Sansigre A., Rawlings S., Lacy M., Fadda D., Jarvis M.J., Marleau F.R., Simpson C., Willot C.J., 2006a, MNRAS, 370, 1479
 Miley G., De Breuck C., 2008, A&ARv, 15, 67
 Morganti R., Garrett M.A., Chapman S., Baan W., Helou G., Soifer T., 2004, A&A, 424, 371
 Overzier R. A., Miley G. K., Ford H. C., 2007, NewAR, 51, 202
 Pentericci L., Roettgering H. J. A., Miley G. K., Carilli C. L., McCarthy P., 1997, A&A, 326, 580
 Polletta M., et al., 2006, ApJ, 642, 673
 Polletta M., et al., 2007, ApJ, 663, 81
 Pope A., et al., 2006, MNRAS 370, 1185
 Pope A., et al., 2008, ApJ, 689, 127
 Rieke G. H., Alonso-Herrero A., Weiner B. J., Pérez-González P. G., Blaylock M., Donley J. L., Marcillac D., 2009, ApJ, 692, 556
 Rigby E. E., Snellen I. A. G., Best P. N., 2007, MNRAS, 380, 1449
 Sawicki M., & Webb T.M.A., 2005, ApJ, 618, L67
 Schawinski K. et al., 2006, Nature, 442, 888
 Shen Y., et al., 2007, AJ, 133, 2222

- Vega O., Clemens M. S., Bressan A., Granato G. L., Silva L., Panuzzo P., 2008, *A&A*, 484, 631
- Venemans B. P., et al., 2007, *A&A*, 461, 823
- Yan L., et al., 2005, *ApJ* 628, 604
- Yan L., et al., 2007, *ApJ* 658, 778
- Younger J.D., et al., 2007, *ApJ* 671 1531
- Yun M.S., et al., 2008, *MNRAS*, 389, 333
- Webb T.M.A., Lilly A.J., Clements D.L., Eales S., Yun M., Brodwin M., Dunne L., Gear W.K., 2003, *ApJ* 597, 680
- Weedman D.W., Le Flo'ch E., Higdon S.J.U., Higdon J.L., Houck J.R., 2006a, *ApJ* 638, 613
- Weedman D.W., et al., 2006b *ApJ* 653, 101
- West M., 1994, *MNRAS* 268, 79
- Zylka R., 1998, Pocket Cookbook for the MOPSI software in www.iram.es/IRAMES/otherDocuments/manuals/Datared/pockcoo.ps (IRAM, Grenoble)